



OPEN ACCESS

EDITED BY
Tianchen He,
Hohai University, China

REVIEWED BY
Licheng Wang,
Institute of Tibetan Plateau Research
(CAS), China
Dawei Lv,
Shandong University of Science and
Technology, China

*CORRESPONDENCE
Shuo Cao,
✉ caoshuo@cugb.edu.cn
Jing Ma,
✉ mj15501273256@163.com

SPECIALTY SECTION
This article was submitted to
Biogeoscience,
a section of the journal
Frontiers in Earth Science

RECEIVED 11 January 2023
ACCEPTED 23 January 2023
PUBLISHED 03 February 2023

CITATION
Cao S, Ma J and Zhang L (2023),
Quantitative reconstruction of Early
Cretaceous dune morphology in the
Ordos paleo-desert and its
paleoclimatic implications.
Front. Earth Sci. 11:1142034.
doi: 10.3389/feart.2023.1142034

COPYRIGHT
© 2023 Cao, Ma and Zhang. This is an
open-access article distributed under the
terms of the [Creative Commons
Attribution License \(CC BY\)](#). The use,
distribution or reproduction in other
forums is permitted, provided the original
author(s) and the copyright owner(s) are
credited and that the original publication in
this journal is cited, in accordance with
accepted academic practice. No use,
distribution or reproduction is permitted
which does not comply with these terms.

Quantitative reconstruction of Early Cretaceous dune morphology in the Ordos paleo-desert and its paleoclimatic implications

Shuo Cao^{1*}, Jing Ma^{2*} and Laiming Zhang¹

¹State Key Laboratory of Biogeology and Environmental Geology, and School of Earth Sciences and Resources, China University of Geosciences (Beijing), Beijing, China, ²Institute of Mineral Resources Research, China Metallurgical Geology Bureau, Beijing, China

Deserts are among the most important terrestrial sedimentary environments and have existed in all periods throughout Earth's history. In contrast to modern deserts, the ability to quantitatively evaluate the area and desertification degrees of ancient deserts is limited due to the lack of unambiguous proxies. Dune morphology and their spatial arrangements directly reflect the degree of desertification of deserts. Recently, a methodology for obtaining the morphological parameters of dunes was established, although it has not been applied to ancient dunes and deserts in deep time. In the Ordos Basin, both the Early Cretaceous desert and modern deserts (Hobq Desert and Mu Us Desert) were well developed and exposed, which makes the Ordos Basin an ideal place to quantitatively evaluate the paleo-desert based on the proposed methodology. In this study, a total of 698 and 1,490 morphological parameters reflecting the Early Cretaceous desert and modern deserts in the Ordos Basin were obtained, respectively. For the Ordos paleo-desert, our results show that its area was larger and its degree of desertification was more severe than those of modern mid-latitude deserts, including the modern desert in the Ordos Basin, but were similar to those of the modern low-latitude deserts. Our results, therefore, suggest that the Ordos paleo-desert was a non-negligible and large desert during an interval of Earth's history. Since the other controlling factors, such as regional geography and sources of both the ancient and modern deserts in the Ordos Basin, have remained nearly unchanged, we speculate that it may have been the relatively high temperature, high levels of atmospheric carbon dioxide and relatively low precipitation during the greenhouse period (i.e., Early Cretaceous) that led to the large area and severe degree of desertification of the Ordos paleo-desert.

KEYWORDS

Ordos paleo-desert, quantitative dune morphology, Hobq Desert and Mu Us Desert, Early Cretaceous, greenhouse climate

1 Introduction

Deserts are among the most important terrestrial sedimentary environments, and their sedimentary records extend throughout Earth's history (Mountney, 2006; Rodríguez-López et al., 2014). Modern deserts are compared and evaluated mainly by their area and degree of desertification (degree of sand cover) (Laity, 2009; Pye, 2009). However, due to the lack of unambiguous proxies, the ability to quantitatively evaluate ancient deserts in geological history and explore their formation mechanisms is limited (Cosgrove et al., 2021a; Cosgrove et al., 2021b; Cosgrove et al., 2021c; Rodríguez-López et al., 2014).

Dunes are the primary landforms in deserts (Mountney, 2006; Laity, 2009). Their morphology and spatial arrangement directly reflect the degree of desertification and serve as an ideal proxy to quantitatively evaluate deserts (Dong et al., 2009; Al-Masrahy and Mountney, 2013). Recently, a methodology was established by Ma et al. (2021) to measure and calculate the morphological parameters of ancient dunes, which further enables the quantitative descriptions of dune morphology in deep time. However, its applicability has not been verified.

Previous sedimentological studies proved that an Early Cretaceous desert (paleo-desert for short) was well developed and exposed across the entire Ordos Basin, northern China (Qi and Li, 1996; Jiang et al., 2004; Qiao et al., 2021). In this study, we measure and calculate 698 morphological parameters of 241 ancient dunes in the Ordos paleo-desert. After comparing the dune morphological parameters of modern deserts (Hobq Desert and Mu Us Desert) in the Ordos Basin and other typical modern deserts all over the world, our results suggest that the area was larger and the degree of desertification was more severe in the Ordos paleo-desert than in the modern mid-latitude deserts, including the modern desert in the Ordos Basin, but similar to those of the modern low-latitude deserts. We speculate that the typical greenhouse climate led to the large area and severe desertification that occurred within the Ordos paleo-desert during the Early Cretaceous.

2 Geological setting

The Ordos Basin, also known as the Ordos Plateau, is a highland sedimentary basin in Northwest China with an elevation of 1,000–1,600 m. It is the second largest sedimentary basin in China and has a total area of 370,000 km² (Liu and Yang, 2018; Zhang et al., 2020). The basin is bounded to the east by the Lvliang and Taihang Mountains, to the north by the Yin Mountains, to the west by the Helan Mountains, and to the south by the Qinling Orogen (Shi et al., 2020; Figure 1). Since the Early Cretaceous, the location of the Ordos Basin has basically remained unchanged (at 34°N–41°N, 104°E–112°E) (Jiang et al., 2001). Two modern deserts (Yang et al., 2012) and a paleo-desert (Qiao et al., 2021) developed in the Ordos Basin.

The modern deserts are confined to the northern part of the Ordos Basin. It comprises two deserts: the Hobq Desert in the north and the Mu Us Desert in the south (Liu and Yang, 2018). The Hobq Desert (107°08'–111°30' E, 39°40'–40°48' N), formed in the Early Holocene, extends ~300 km from west to east, and its width decreases from ~100 km in the west to 20–30 km in the east, covering an area of 16,000 km² (Sun et al., 2006; Yang et al., 2016). Most of the area is covered by desert landscapes, characterized by crescentic dunes (Fan et al., 2013; Xu et al., 2018). The Mu Us Desert (106°11'–110°54' E, 36°49'–40°12' N), which formed in the Late Pleistocene, has an area of ~39,000 km² and a dune field area of 34,033 km² (He et al., 2010). The

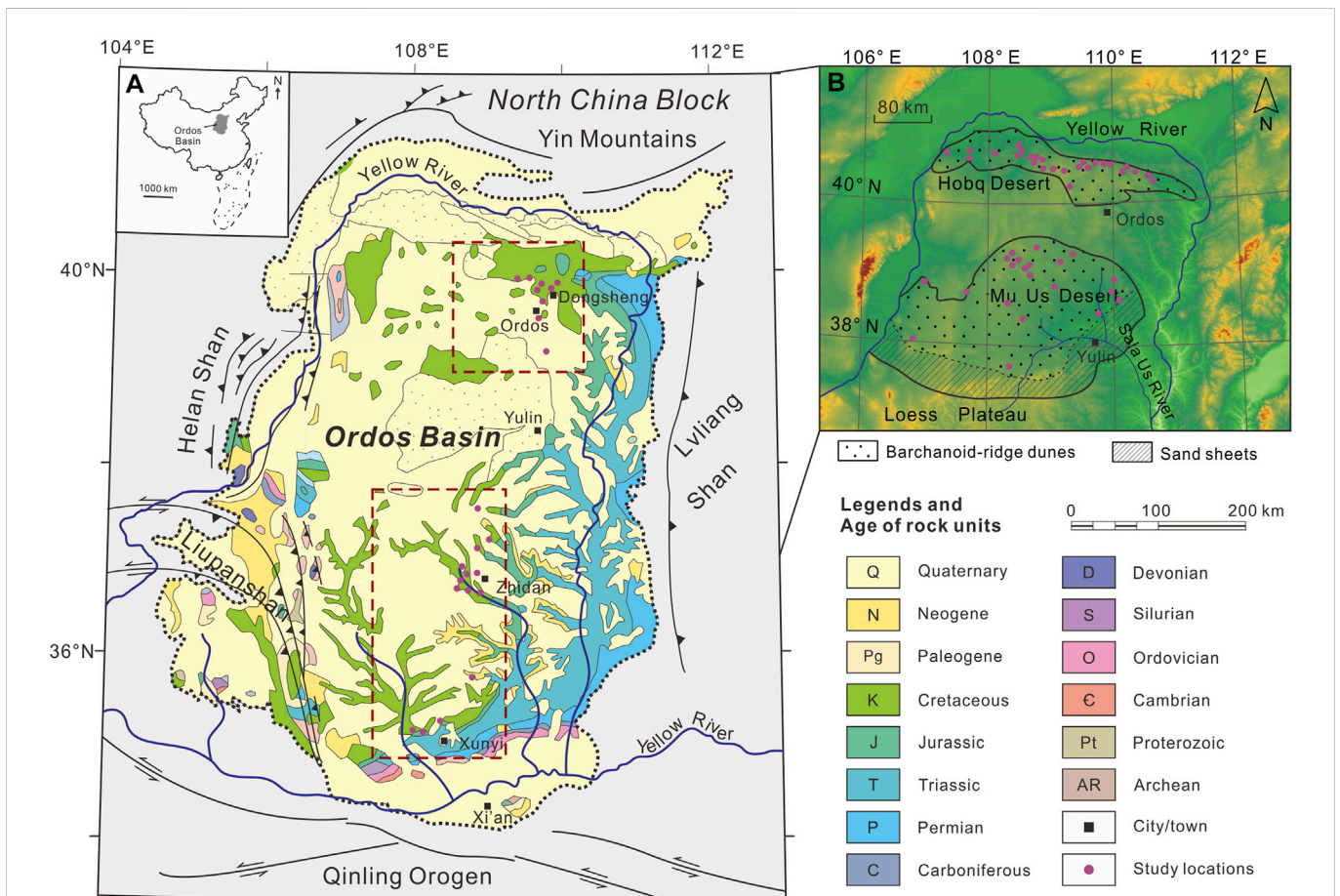


FIGURE 1 (A) Geological map of the Ordos Basin. (B) Digital Elevation Model (DEM) of the modern deserts (Hobq Desert and Mu Us Desert) in the Ordos Basin. Dashed box: study area; circle: data measurement outcrop locations.

TABLE 1 Summary of morphological parameters of aeolian dunes (Al-Masrahy and Mountney, 2013; Romain and Mountney, 2014).

Type	Morphological parameter (Code)	Description	Equation
Macro-parameter	Dune height (H)	The difference in relief between the crest of a bedform and the general level of the desert surface where interdune flats are present	
	Dune spacing (SP)	The crest-to-crest (or toe-to-toe) distance between adjacent bedforms in an orientation perpendicular to the trend of elongate bedform crestlines	$H = 0.12Sp$
	Dune wavelength (DW)	The distance from the leeward toe to the rearward (stoss) toe of the bedform in an orientation parallel to the direction of downwind migration	$SP=DW$ (central-desert)
	Dune wave width (WA)	The wavelength of along-crest sinuosity of dune	$WA=11.29H$
Micro-parameter	Grain-flow thickness (t)	The thickness of grain-flow strata arising from individual lee slope sand avalanches, a function of the length of the lee slope of the original bedform down which avalanching grains of sand cascaded to generate the deposit. It represents single grain flow events	$H = 988.78t^{1.4796}$
Indirect-parameter	Preserved set thickness (λ)	Originated <i>via</i> bedform climbing and records the thickness of one period of accumulation, a function of both original bedform wavelength and the angle at which the bedforms climbed over one another as accumulation proceeded	$DW = \lambda/\tan \Phi$
	Angle of set climb (Φ)	The dip angle of the interdune migration plane relative to the underlying suppersurface	
	Slipface horizontal length (L)	Horizontal component of the distance projected from the top of the dune to the bottom of the leeward slope	$H = L \cdot \tan \alpha$
	Angle of repose (α)	The minimum angle to the horizontal surface at which slipface causes sand to be in the critical state of sliding along the inclined surface	

inner Mu Us Desert is mainly composed of semistabilized barchanoid-ridge dunes (Wang et al., 2017). However, in the southern marginal Mu Us Desert, the sand-loess transitional zone, i.e., the main geomorphic units, are discontinuous sand sheets (Sun, 2000; Huang et al., 2009).

In contrast to modern deserts, the paleo-desert covered almost the entire Ordos Basin during the Early Cretaceous (~142–136 Ma, Berriasian-Valanginian) (Deng et al., 2008; Huang, 2010; Qiao et al., 2021). The aeolian strata in the Ordos Basin are mainly developed in the Luohe and Luohandong Formations (Jiang et al., 2001; Xing et al., 2018). Here, our study is focused on the typical paleo-desert deposits in the Luohe Formation, which has an area of 370,000 km² (Jiang et al., 2004). The aeolian sequences in this formation have an average thickness of 110–430 m and are mainly exposed in the middle and western parts of the basin (Deng et al., 2008; Zhu et al., 2018). The dune deposits are well developed and preserved (Qiao et al., 2021).

3 Methods

3.1 Morphological parameter of dunes

As mentioned above, the dune morphology could be quantitatively described by morphological parameters, including height (H), spacing (SP), wavelength (DW), wave width (WA), average thickness of grainflow strata (t), preserved set thickness (λ), climbing angle (Φ), horizontal length of slipface (L), and angle of repose (α) (Table 1; Al-Masrahy and Mountney, 2013; Mountney and Howell, 2000; Romain and Mountney, 2014; Yang H et al., 2019). Among these parameters, DW , WA , and H (similar to the length, width, and height) together can directly reflect the size of a dune and are used for comparison. For modern dunes, SP , DW , WA , and L can be directly obtained by field measurement or remote sensing images (Al-Masrahy and Mountney,

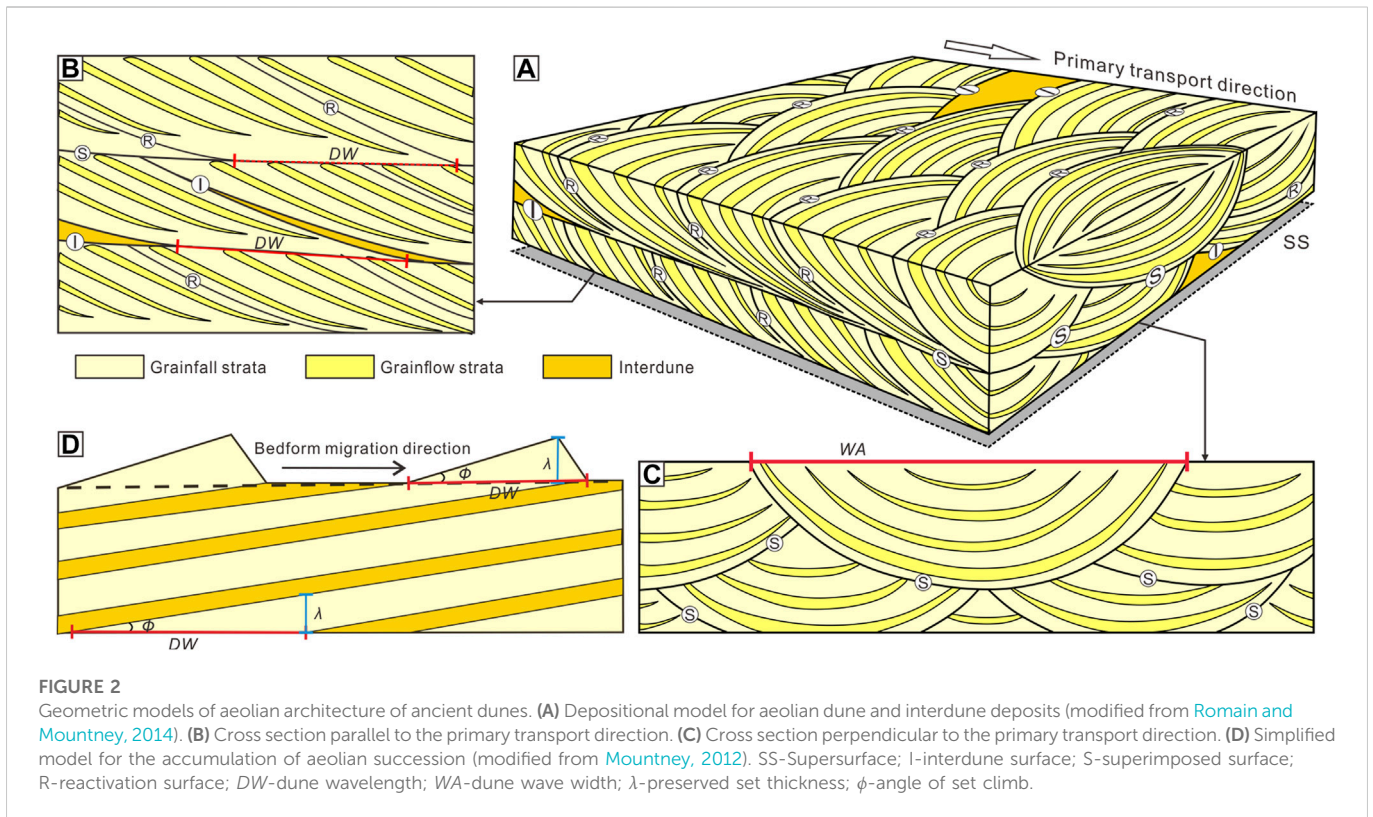
2013). For ancient dunes, SP , DW , WA , t , λ , and Φ can be directly obtained by field measurement if the outcrops are well exposed and well preserved (Mountney, 2012; Romain and Mountney, 2014). The other parameters can be indirectly calculated based on the above parameters (Yang J et al., 2019; Ma et al., 2021; Junhuai).

3.2 Measurement of morphological parameters

A total of 434 data points were measured from 241 dunes from the paleo-desert, and a total of 653 and 484 data points were measured from 215 to 160 dunes from the Hobq and Mu us Deserts, respectively. Dunes can be divided into many types, for example, crescentic, transverse, linear, and star (Mountney, 2006). Among them, crescentic dunes are simple in structure and widely distributed. During the process of long-distance migration, the size and shape of sediment in crescentic dunes do not significantly change (Ma et al., 2021). Therefore, to ensure the accuracy of our measurements, only simple and compound crescentic dunes were measured in this study (Xiao, 2017).

3.2.1 Ancient dunes in the Luohe Formation

The outcrops of the Luohe Formation are well preserved and fully exposed, which facilitates measurement. The outcrops at Dongsheng, Zhidan, and Xunyi (Figure 1) are accessible, well exposed, and laterally extensive, and their planar cliff faces are oriented either parallel or perpendicular to the paleowinds (Jiang et al., 2001; Qiao et al., 2021). According to the accumulation mechanism of climbing aeolian systems, all the morphological parameters should be measured in the section as close to parallel or perpendicular to the paleowinds as possible since oblique sections make the measurements larger or smaller (Mountney, 2012; Romain and Mountney, 2014; Figure 2).



(1) DW . DW is the distance between two successive interdune deposits in the sections that were (nearly) parallel to the paleowinds (Mountney and Howell, 2000; Figure 2B, Figure 3A). If the interdune deposits are absent, then the superimposed surfaces instead of the interdune surfaces can be used, but this will lead to a smaller value than the actual value (Figure 2B, Figure 3B). In the desert center, SP is approximately equal to DW , as interdunes are not developed (Ma et al., 2021).

(2) WA . WA is the distance between the wings of trough cross-bedding in the sections that were (nearly) perpendicular to the paleowinds (Ma et al., 2021; Figure 2C, Figures 3C, E).

(3) ϕ , λ . ϕ and λ need to be measured together from compound crescentic dune deposits (Mountney and Howell, 2000). ϕ is the angle between the climbing surface of dunes and the supersurface (Mountney, 2012; Figure 2D). The generally horizontal strata of the Luohe Formation indicate that the supersurface is also horizontal (Xue et al., 2010). In this case, ϕ is the dip of the superimposed surfaces in the section (nearly) parallel to the paleowinds (Figure 3F). λ is the vertical distance of two adjacent superimposed surfaces in sections parallel or perpendicular to the paleowinds (Figure 2D, Figure 3F).

(4) t . For sections either perpendicular or parallel to the paleowinds, a t series consists of the measurements of the grain flow unit lamina by lamina in one cross-bedded dune set (Howell and Mountney, 2001; Romain and Mountney, 2014; Figure 3D).

In total, for ancient dunes in the Luohe Formation, 144 DW , 74 WA , 23 sets of ϕ and λ , and 170 t (7 sets) are measured (Supplementary Table S1).

3.2.2 Modern dunes in the Hobq and Mu Us Deserts

The measurement of modern dune morphological parameters is much easier (Al-Masrahy and Mountney, 2013). Based on the satellite imagery provided by Google Earth Pro software and datasets of the Hobq and Mu Us Deserts, DW , WA , and L can be measured directly for dunes without vegetation cover (Figure 4). For a dune, DW is measured from its leeward toe to its rearward toe in an orientation parallel to the migration direction, WA is measured from one wing to the other, and L is measured as the horizontal length of its lee slope. In addition, the dune morphological parameters of the Hobq and Mu Us Deserts reported by previous studies are also compiled (Du et al., 2011; Du et al., 2013; Wang et al., 2013; Zhang, 2019; Xu et al., 2020).

In total, for modern dunes in the Hobq Desert, 215 DW , 206 WA , and 214 L were obtained. For modern dunes in the Mu Us Desert, 160 DW , 160 WA , and 160 L were obtained (Supplementary Table S2).

3.3 Calculation of the unmeasurable morphological parameters

As we have mentioned above, we use DW , WA , and H to make comparisons. In contrast to WA , H for both ancient and modern dunes and DW for part of ancient dunes cannot be directly measured due to the relatively bad outcrop conditions (Mountney, 2006). Fortunately, according to previous studies, there are mathematical relationships between H and SP , H and t , and H and WA for simple and compound crescentic dunes (Hesp and Hastings, 1998; Howell and Mountney, 2001; Dong et al., 2009; Romain and Mountney, 2014). Ma et al. (2021) summarized these empirical equations as follows.

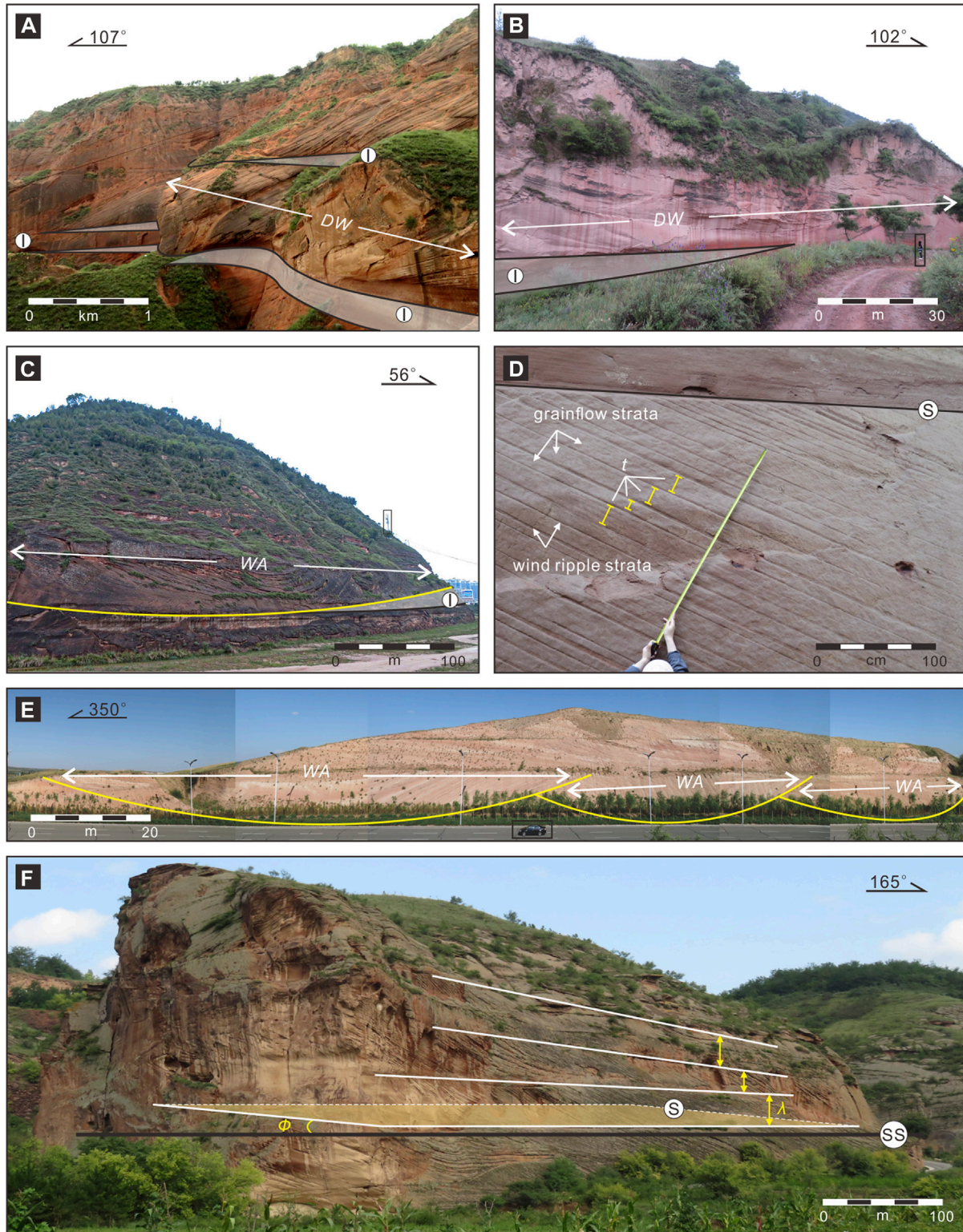


FIGURE 3

Outcrops of morphological parameters of ancient dunes. (A) Dune deposit bounded on both sides by interdune deposits in the section nearly parallel to the paleowind. (B) Dune deposit bounded on one side by interdune deposit in the section nearly parallel to the paleowind. (C) Large-scale aeolian though cross-bedding with interdune deposits in the section nearly perpendicular to the paleowind. (D) Detail of aeolian cross-bedding showing grainflow and grainfall lamination. (E) A series of cross-beddings in the section perpendicular to the paleowind. (F) Large-scale compound aeolian dunes in the paleo-desert center. SS-Supersurface; I-interdune surface; S-superimposed surface; DW-dune wavelength; WA-dune wave width; t -grain flow thickness; λ -preserved set thickness; ϕ -angle of set climb.

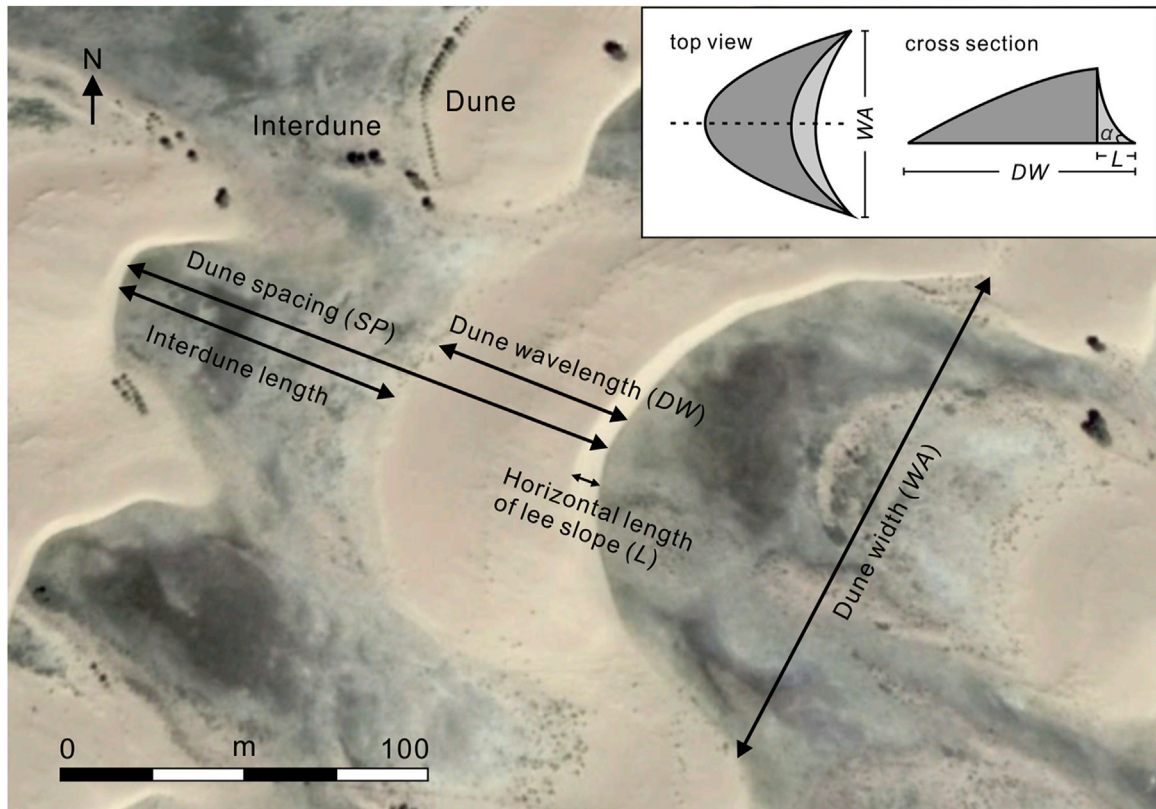


FIGURE 4 Remote-sensing image of dune and interdune of the Hobq Desert, including definitions of the terminology used in this study to quantitatively describe their morphology and geometry. Sketch map in top view and cross section of a dune is at the top right. H -original dune height; L -horizontal length of dune slipface; α -angle of repose.

$$H = a_1 Sp^{b_1} \tag{1}$$

$$H = a_2 t^{b_2} \tag{2}$$

$$WA = a_3 H + c_1 \tag{3}$$

$$H = 0.12Sp \tag{6}$$

$$H = 0.12DW \tag{7}$$

$$WA = 11.29H \tag{8}$$

$$H = 988.78t^{1.4796} \tag{9}$$

In these equations, a_1 , a_2 , and a_3 are coefficients, b_1 and b_2 are the numbers of occurrences, and c_1 is a constant. The values of a_1 , a_2 , b_1 , b_2 , and c_1 mainly depend on the internal and external features of deserts, such as sand properties, surface morphology, wind field, and terrestrial vegetation (Ma et al., 2021). In addition, based on the geometry of dune deposits (Figure 2D, Figure 4), the conversion equations for H , L and α , and DW , λ and ϕ are as follows (Mountney and Howell, 2000; Yang H et al., 2019).

$$H = L \tan \alpha \tag{4}$$

$$DW = \lambda / \tan \phi \tag{5}$$

By analyzing the properties of mid-latitude modern and ancient desert deposits, previous studies have suggested that the paleo-desert shares similar characteristics with the Badain Jaran Desert, the Kumtag Desert and the Permian Cedar Mesa Sandstone deposits (Dong et al., 2009; Rodríguez-López et al., 2014; Romain and Mountney, 2014; Liu and Yang, 2018). Therefore, based on Eqs 1–3, the following empirical equations derived from the Badain Jaran Desert and the Kumtag Desert and Eq. 5 are used to calculate the unmeasurable DW and H for the ancient dunes of the paleo-desert (Dong et al., 2009; Ren et al., 2010; Romain and Mountney, 2014).

As SP approximately equals DW in the desert center, Eq. 7 can only be applied in the desert center. By using Eqs 5–9, 23 DW and 241 H are calculated for the paleo-desert. To validate our calculations, we measure DW and t and WA and t of the same dune and then calculate H by both Eqs 7, 8 and Eqs 7, 9. The results for H of the different equations are consistent.

In Eq. 4, α is a dynamic equilibrium state shaped by the interaction of regional terrain, wind, and sand sources (Yang J et al., 2019). Wang et al. (2017) measured an α of 32° in the Hobq Desert and the Mu Us Desert. Based on L obtained from the remote sensing images, 197 and 156 H are calculated in the Hobq Desert and the Mu Us Desert, respectively (Supplementary Table S2).

4 Results

Table 2 summarizes the results of the statistical analysis of DW , WA , and H of both ancient dunes in the paleo-desert and modern dunes in the Hobq Desert and the Mu Us Desert in the Ordos Basin.

TABLE 2 Results of statistical analysis of wavelength (DW), wave width (WA) and height (H) of both the ancient and modern dunes in the Ordos Basin.

Location	Morphological parameter	Statistical analysis					
		Number	Maximum (m)	Minimum (m)	Mean (m)	Standard deviation	Coefficient of variance
paleo-desert center	DW	83	2,252	105	562	493	88
	WA	25	523	135	308	115	37
	H	108	270	12	58	55	94
paleo-desert margin	DW	84	270	36	98	45	46
	WA	49	201	52	100	38	38
	H	133	32	4	11	5	59
Hobq Desert	DW	215	262	27	90	39	43
	WA	206	315	38	119	50	42
	H	215	23	1	9	5	51
Mu Us Desert	DW	160	233	38	90	38	42
	WA	160	373	40	149	61	41
	H	160	26	1	10	5	48

*All the statistical dunes are simple and compound crescentic dunes.

The evolution of *DW*, *WA*, and *H* from the desert center to the desert margin is shown in [Figure 5](#).

4.1 The Hobq Desert

The Hobq Desert covers an area of 16,000 km² ([Sun et al., 2006](#); [Yang et al., 2016](#)). A total of 215 dunes have been analyzed in the Hobq Desert. Most of the Hobq Desert is covered by active crescentic dunes and sandsheets ([Figure 5A](#)). In the Hobq Desert, *DW* ranges from 27 m to 262 m with an average value of 90 m. *WA* ranges from 38 m to 315 m with an average value of 119 m. *H* ranges from 1 m to 23 m with an average value of 9 m ([Table 2](#)).

According to the fitting curves in [Figure 5B](#), *DW*, *WA* and *H* are distributed discretely with high standard deviation in the Hobq Desert. From the desert center to the desert margin, there is no obvious variation in dune size across the desert ([Figure 5A](#)).

4.2 The Mu Us Desert

The Mu Us Desert covers an area of ~39,000 km² ([He et al., 2010](#)). A total of 160 dunes have been analyzed in the Mu Us Desert. Active and stabilized dune fields within the Mu Us Desert developed on the Mesozoic bedrock in the eastern and southern regions of the desert ([Figure 5B](#)). The Mu Us Desert is a steppe desert characterized by mobile, semimobile, and semifixed dunes with a mosaic structure similar to loess grasslands. In the Mu Us Desert, *DW* ranges from 38 m to 233 m with an average value of 90 m. *WA* ranges from 40 m to 373 m with an average value of 149 m. *H* ranges from 1 m to 26 m with an average value of 10 m ([Table 2](#)).

[Figure 5B](#) shows that *DW*, *WA*, and *H* decrease gradually moving away from the desert center to the desert margin, but the decreasing trend is not significant. The ranges in the variability of *DW*, *WA*, and *H* are relatively limited, and most of the dunes in the Mu Us Desert are relatively small.

4.3 Paleo-desert in the Ordos Basin

The paleo-desert covers the entire basin with an area of 370,000 km² ([Qiao et al., 2021](#)) ([Figure 5C](#)). It consists of typical desert center and margin subenvironments. For the paleo-desert margin, *DW* ranges from 36 m to 270 m with an average value of 98 m. *WA* ranges from 52 m to 201 m with an average value of 100 m. *H* ranges from 4 m to 32 m with an average value of 11 m ([Table 2](#)). For the paleo-desert center, *DW* ranges from 105 m to 2,252 m with an average value of 562 m. *WA* ranges from 135 m to 523 m with an average of 308 m. *H* ranges from 12 m to 270 m with an average of 58 m ([Table 2](#)). In the desert center (0–60 km), *DW*, *WA*, and *H* increase dramatically and gradually decrease to the paleo-desert margin. Notably, a series of mega-dunes that are 2,252 m long, 523 m wide, and 270 m high were formed in the paleo-desert center ([Figure 5C](#)).

The maximum *DW* and *H* of the paleo-desert are up to 9–12 times those of the Hobq Desert and Mu Us Desert ([Table 2](#); [Figure 6A](#)). Even the mean *DW* and *H* of the paleo-desert are approximately 4 times those of the Hobq Desert and Mu Us Desert ([Table 2](#); [Figure 6A](#)). However, the maximum and mean *WA* values of the paleo-desert are no more than twice those of the Hobq and Mu Us Deserts, respectively ([Table 2](#); [Figure 6A](#)). We speculate that the *WA* of the paleo-desert may have been underestimated due to the limited preservation conditions.

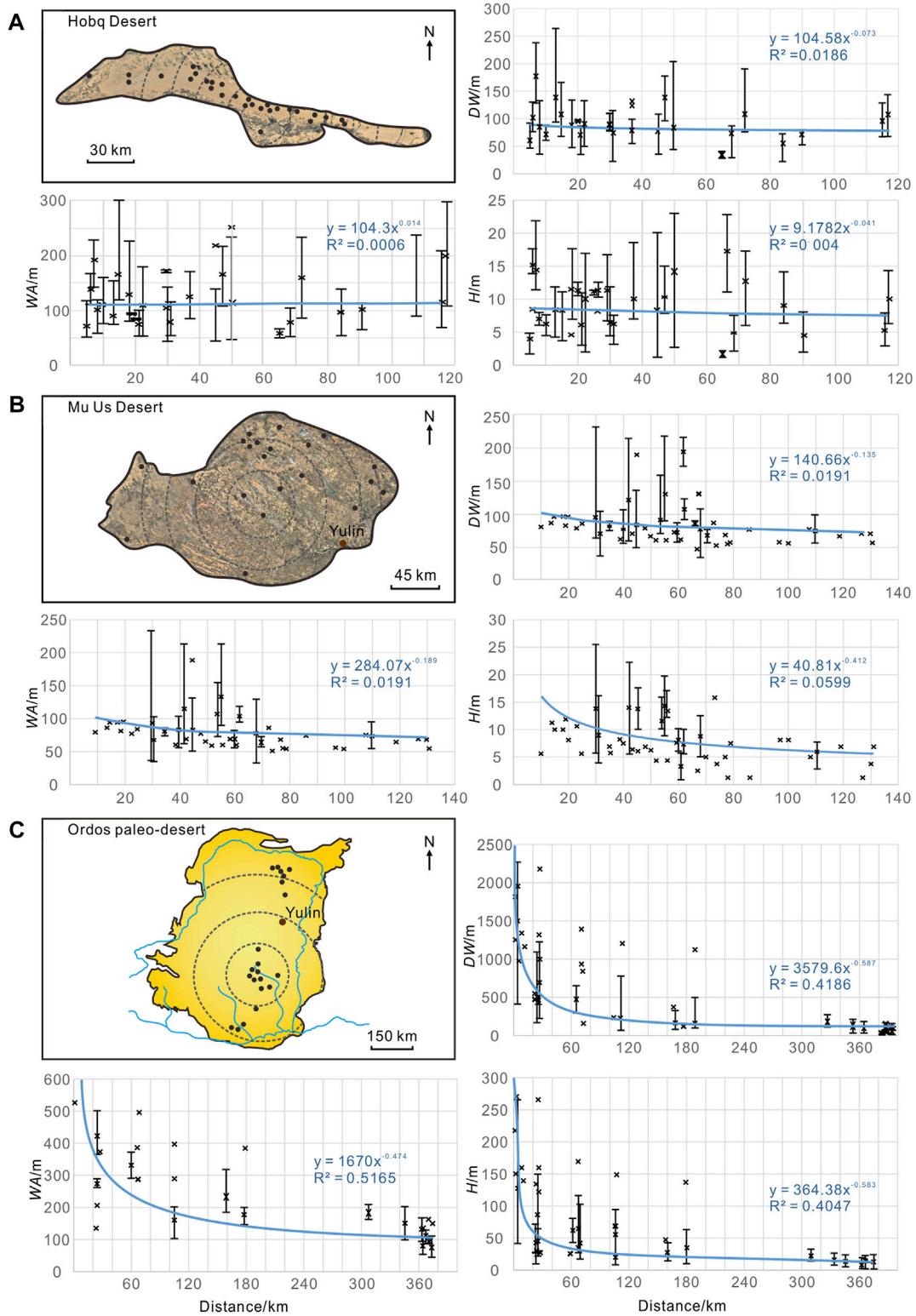
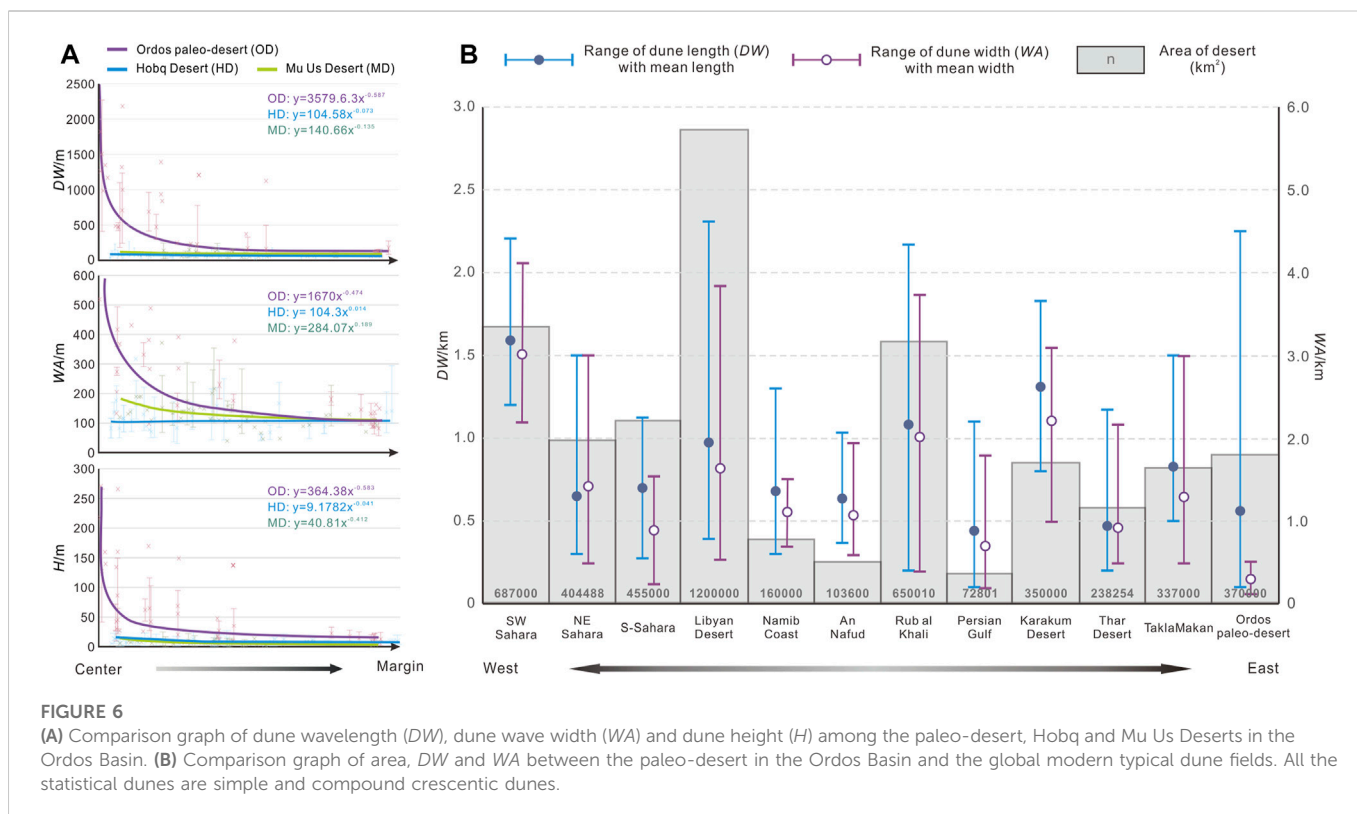


FIGURE 5 Outline map and graph of dune wavelength (*DW*), dune wave width (*WA*) and dune height (*H*) against distance from the desert center in the Hobq Desert (A), Mu Us Desert (B), and paleo-desert (C) in the Ordos Basin. The dotted circle (from the center to the boundary) corresponds to the center of the desert to the margin; black circles show locations where data was collected and measurements were taken; blue lines are the fitting curves with the equation of the line and R^2 value also shown. The line segments in the graphs represent the range of values. All the statistical dunes consist of simple and compound crescentic dunes.



5 Discussion and implications

5.1 Quantitative evaluation of the large paleo-desert in the Ordos Basin

During the Early Cretaceous, aeolian deposits covered the entire Ordos Basin and are considered to represent a typical desert environment (Qi and Li, 1996; Li et al., 1999; Qiao et al., 2021). Many sedimentological studies have already been conducted to investigate the paleo-desert, including analyses of desert-related sedimentary facies (Qi and Li, 1996) and reconstruction of aeolian architecture and evolution models (Qiao et al., 2021). These studies indicated that the paleo-desert in the Ordos Basin was a large sandy desert, but no quantitative constraints have been made.

In general, deserts can be quantified and evaluated in different aspects, and the two representative and comparable aspects are the area and degree of desertification (Laity, 2009). As deserts are usually covered by sand and vegetation, the term “desertification” can be defined as a land degradation process and can be reflected by the ratio between the sand cover area and desert area (Pye, 2009; Mirzabaei et al., 2019; Yu et al., 2020). Unlike desert areas, which can be obtained directly, desertification is difficult to quantify, especially in ancient deserts (Laity, 2009). In most cases, desertification is positively correlated with the range of the sizes of the dunes as well as the maximum dune size (Al-Masrahy and Mounthey, 2013; Cosgrove et al., 2021a, b). For example, for each desert, the sizes of its dunes commonly lie within a specific range, although the dune size tends to be smaller in the desert margin and larger in the desert center (Lancaster, 1994; Rubin and Carter, 2006; Ewing and Kocurek, 2010). Therefore, evaluating the dune morphology and dune size

may help to quantify the degree of desertification of each desert. In this study, based on *DW*, *WA*, and *H* (Al-Masrahy and Mounthey, 2013), we quantitatively evaluate the degree of desertification of the Ordos paleo-desert.

Here, the area and degree of desertification of the Ordos paleo-desert are compared with those of the modern deserts (Hobq and Mu Us Deserts) in the Ordos Basin and other typical modern deserts all over the world. First, the area of the Ordos paleo-desert is nearly ten times the total area of the Hobq and Mu Us Deserts (He et al., 2010; Yang et al., 2016; Qiao et al., 2021). The range and maximum size of the dunes of the Hobq and Mu Us Deserts are similar to those of the Ordos paleo-desert margin but are much smaller than those of the Ordos paleo-desert center (Figure 6A). Therefore, our results suggest that both the area and degree of desertification of the Ordos paleo-desert exceed those of the modern deserts in the Ordos Basin. Second, the area of the Ordos paleo-desert is slightly larger than that of the mid-latitude Taklimakan Desert (largest desert in China) and Karakum Desert (largest desert in Central Asia) (Qiao et al., 2021; Rittner et al., 2016; Zonn and Esenov, 2012; Figure 6B). The dune size (i.e., the range and maximum value of *DW*) of the Ordos paleo-desert is larger (Breed and Grow, 1979; Figure 6B), which indicates a more severe degree of desertification in the Ordos paleo-desert than in the Taklimakan Desert and Karakum Desert. Third, although the areas of the low-latitude Sahara Desert in Africa and the Rub’al Khali Desert in the Arabian Peninsula, by far the largest hot deserts on Earth (Pastore et al., 2021; Xiao et al., 2021), are larger than that of the Ordos paleo-desert, the Ordos paleo-desert has a larger dune size (Al-Masrahy and Mounthey, 2013; Breed and Grow, 1979; Figure 6B). This indicates that the degree of desertification in the Ordos paleo-desert was similar to or even more severe than that in the Sahara and Rub’al Khali Deserts.

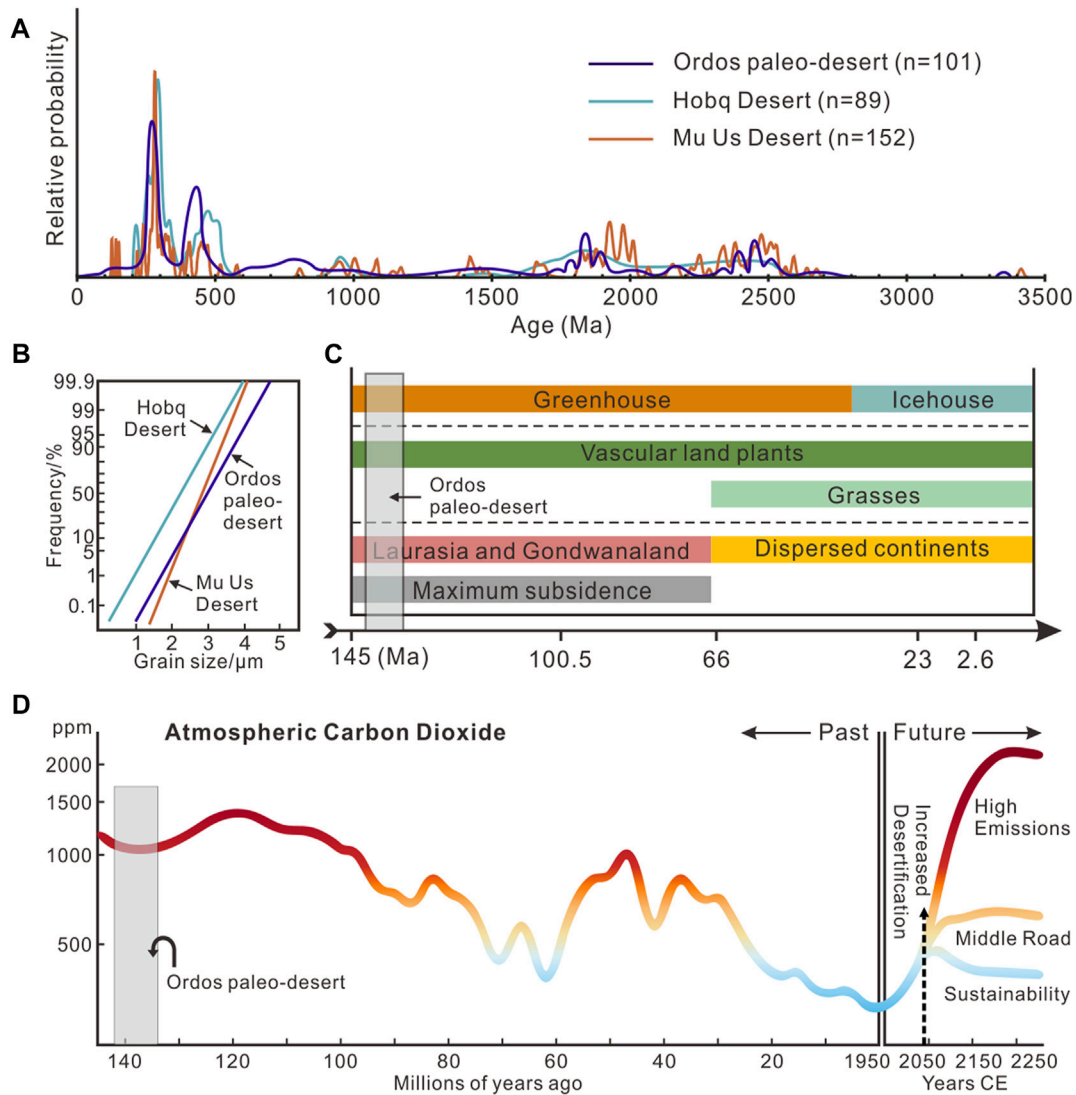


FIGURE 7

(A) U-Pb age spectra of detrital zircons from the Early Cretaceous paleo-desert, Hobq Desert and Mu Us Desert in the Ordos Basin. Data sources: Ordos paleo-desert (Cheng et al., 2020); Hobq Desert (Yang et al., 2017); Mu Us Desert (Stevens et al., 2010). (B) Log-probability cumulative curves of grain-size distribution for aeolian sediments in the Ordos paleo-desert, Hobq and Mu Us Deserts. Data sources: Ordos paleo-desert and Mu Us Desert (Li et al., 1999); Hobq Desert (Zhang et al., 2018). (C) Climate, vegetation, basin subsidence and supercontinental setting governing aeolian construction, accumulation, and preservation from the Cretaceous to the present. Adapted from Cosgrove et al. (2021c). (D) Past carbon dioxide concentrations (left) compared to possible future emissions scenarios (right). Adapted from Tierney et al. (2020) and Meinhausen et al. (2020).

In summary, the comparisons demonstrate that the Ordos paleo-desert was a large and non-negligible desert at one point in Earth's history. The area and degree of desertification of the Ordos paleo-desert exceeded those of the modern deserts in the Ordos Basin and the modern Karakum and Taklimakan Deserts at middle latitudes and was similar to those of the great Sahara and Rub' al Khali Deserts at low latitudes. We suggest that quantitative assessments of dune morphological parameters are useful for evaluating ancient deserts in deep time.

5.2 The controlling factors on the formation, development, and evolution of deserts

Deserts developed both in the modern era and the Early Cretaceous in the Ordos Basin (Liu and Yang, 2018; Qiao et al.,

2021). According to the quantitative data of the desert area and the dune morphology, the paleo-desert is much larger than the modern deserts in the Ordos Basin (Figure 5, Figure 6A). The formation of deserts is generally controlled by internal factors (e.g., basin properties) and external factors (e.g., geomorphic and geographic conditions, potential source area and sediment features, the evolution of terrestrial plants, and climate conditions) (Mountney, 2006; Lu et al., 2019; Cosgrove et al., 2021b; Zhu et al., 2021). These controlling factors are discussed below.

The Ordos Basin is a large intracratonic depression in the western part of the North China Block, and it underwent multistage modification during the Mesozoic (Zhao et al., 2020). By identifying the deposits of the marginal alluvial fan facies, since the Late Jurassic, the eastern, western, southern, and northern boundaries of the Ordos Basin have been roughly confined by the Taihang (Li

et al., 2015) and Helan Mountains (Yang and Dong, 2018) and Qinling Orogen (Dong et al., 2011) and Yin Mountains (Xiao et al., 2018), respectively. Therefore, the paleogeographic configuration of the mountains surrounding the Ordos Basin has been consistent since the Late Jurassic, forming a rain shadow area in the basin and promoting the development of ancient and modern deserts (Laity, 2009; Zhao et al., 2020). However, the subsidence rates of the Ordos Basin were relatively higher during the Cretaceous, which allowed aeolian bedforms to climb at steeper angles and led to thicker aeolian sequences, but had no effect on the desert area and degree of desertification (Cosgrove et al., 2021b, 2022; Figure 7C).

With respect to the provenance of the Ordos paleo-desert and modern deserts, previous studies have suggested that detrital zircon U–Pb ages show the same peaks at ~280 Ma, ~450 Ma, ~960 Ma, ~1,900 Ma, and ~2,500 Ma (Cheng et al., 2020; Stevens et al., 2010; Yang et al., 2017; Figure 7A). The detrital zircon age spectra indicate that the ancient and modern deserts in the Ordos Basin have abundant sand supplies and that their source areas are similar, consisting of the surrounding mountains and some distant sediments (Stevens et al., 2010; Yang et al., 2017; Cheng et al., 2020). In addition, the aeolian sands in the Ordos paleo-desert and the modern deserts also share similar sediment features, such as similar composition, particle size, and roundness (Li et al., 1999; Zhang et al., 2018; Figure 7B). However, the vegetation of the ancient and modern deserts in the Ordos Basin is slightly different. During the Early Cretaceous, most of the vegetation in the Ordos Basin consisted of vascular land plants, as grasses did not evolve until ca. 66 Ma (Boyce and Lee, 2017; Figure 7C). At present, grasses have become the major vegetation type in the region, play a crucial role in dune construction and stabilization (Cosgrove et al., 2021b), and decrease desertification to some extent.

Climate commonly refers to the long-term regional or global average of temperature, precipitation, wind, and atmospheric carbon dioxide (Pörtner et al., 2022). The modern deserts in the Ordos Basin are in the subtropical high-pressure belt and affected by both the East Asian winter monsoon and westerly circulation patterns (Lü et al., 2020; Yang et al., 2021). At present, in the Ordos Basin, the mean annual temperature is 6°C–8.5°C, the mean annual precipitation is 250–500 mm/year (Liu et al., 2018; Yang J et al., 2019), and the atmospheric carbon dioxide is ~400 ppm (Meinshausen et al., 2020; Figure 7D). However, the Ordos paleo-desert was in the subtropical high-pressure belt and mainly affected by westerlies (Jiang et al., 2001; Qiao et al., 2021). During the Early Cretaceous, the sea-surface temperature was 20°C–25°C (O'Brien et al., 2017), the mean annual precipitation was 190–320 mm/year (Pan and Huang, 2014), and the atmospheric carbon dioxide was ~1,000 ppm (Tierney et al., 2020; Figure 7D). According to the climate parameters, the ancient and modern deserts in the Ordos Basin both had sufficient and similar wind supplies. Based on the location of the Ordos Basin in the subtropical arid belt, the temperature, precipitation and atmospheric carbon dioxide in the Early Cretaceous and modern era are all suitable for the formation of deserts as well (Laity, 2009; Mirzabaev et al., 2019). However, the paleotemperature and the paleo-CO₂ were much higher and the paleo-precipitation was relatively lower when the paleo-desert was formed. The greenhouse climate in the Early Cretaceous may have enlarged the desert area and intensified desertification (Mirzabaev et al., 2019).

In summary, the region was surrounded by mountains, had sufficient sediment source and wind supply, and the suitable climatic conditions promoted the formation of the ancient and

modern deserts in the Ordos Basin. Since all the factors controlling the development of the paleo-desert and modern deserts have basically remained unchanged, with the exception of the climatic conditions, we speculate that the greenhouse paleoclimate during the Early Cretaceous may be the main reason for the relatively large area and relatively severe degree of desertification identified in the Ordos paleo-desert. Though further works are needed to obtain more quantitative dune morphological parameters in deserts with different ages and paleoclimate conditions.

6 Conclusion

Dune morphological parameters provide a new way to quantitatively describe dunes and deserts and provide a basis to evaluate the desertification degrees of deserts. Here, we present the first quantitative assessment of dune morphology and dune size in ancient deserts.

For the Ordos paleo-desert during the Early Cretaceous, the dune size increases dramatically toward the desert center and decreases gradually toward the desert margin. By comparing the desert area and dune morphological data, we statistically demonstrate that the area and degree of desertification of the Ordos paleo-desert exceeded those of the mid-latitude Karakum and Taklimakan Deserts and are similar to those of the low-latitude great Sahara and Rub' al Khali Deserts. The comparison demonstrates that the Ordos paleo-desert was a large and non-negligible desert during an interval of Earth's history. In addition, for the development of the paleo-desert and modern deserts in the Ordos Basin, since all the controlling factors have remained unchanged, with the exception of the climatic conditions, we speculate that the greenhouse paleoclimate during the Early Cretaceous, characterized by high temperatures, high levels of atmospheric carbon dioxide and low precipitation may be the main reason that the Ordos paleo-desert occupied such a relatively large area and had a relatively severe degree of desertification.

Data availability statement

The original contributions presented in the study are included in the article/Supplementary Material, further inquiries can be directed to the corresponding authors.

Author contributions

The author's contributions are shown below: SC: Conceptualization, Data curation, Writing-Original draft preparation; JM: Data curation, Investigation, Visualization; LZ: Writing-Reviewing and Editing.

Funding

This study was financially supported by the National Key R&D Plan of China (grant 2018YFE0204204), the National Natural Science Foundation of China (grant 42102122), and the Fundamental Research Funds for the Central Universities (grants 265202103 and 2652021093).

Conflict of interest

The authors declare that the research was conducted in the absence of any commercial or financial relationships that could be construed as a potential conflict of interest.

Publisher's note

All claims expressed in this article are solely those of the authors and do not necessarily represent those of their affiliated

organizations, or those of the publisher, the editors and the reviewers. Any product that may be evaluated in this article, or claim that may be made by its manufacturer, is not guaranteed or endorsed by the publisher.

Supplementary material

The Supplementary Material for this article can be found online at: <https://www.frontiersin.org/articles/10.3389/feart.2023.1142034/full#supplementary-material>

References

- Al-Masrahy, M. A., and Mountney, N. P. (2013). Remote sensing of spatial variability in aeolian dune and interdune morphology in the Rub' Al-Khali, Saudi Arabia. *Aeolian Res.* 11, 155–170. doi:10.1016/j.aeolia.2013.06.004
- Boyce, C. K., and Lee, J.-E. (2017). Plant evolution and climate over geological timescales. *Annu. Rev. Earth Planet. Sci.* 45, 61–87. doi:10.1146/annurev-earth-063016-015629
- Breed, C. S., and Grow, T. (1979). Morphology and distribution of dunes in sand seas observed by remote sensing. *A study Glob. sand seas* 1052, 253–302.
- Cheng, X., Zhang, T., Miao, P., Cheng, Y., Li, J., Ao, C., et al. (2020). Detrital zircon U-Pb dating from the uranium-bearing sandstone of lower cretaceous of lower segment of Luohe Formation in southwestern Ordos Basin and its peripheral lithospheric extension. *Geol. China*, 1–27.
- Cosgrove, G. I. E., Colomera, L., and Mountney, N. P. (2021a). A database of Aeolian Sedimentary Architecture for the characterization of modern and ancient sedimentary systems. *Mar. Petroleum Geol.* 127, 104983. doi:10.1016/j.marpetgeo.2021.104983
- Cosgrove, G. I. E., Colomera, L., and Mountney, N. P. (2021b). Eolian stratigraphic record of environmental change through geological time. *Geology* 50, 289–294. doi:10.1130/g49474.1
- Cosgrove, G. I. E., Colomera, L., and Mountney, N. P. (2021c). *Quantitative analysis of the sedimentary architecture of eolian successions developed under icehouse and greenhouse climatic conditions*. America: Geological Society of America Bulletin.
- Cosgrove, G. I. E., Colomera, L., and Mountney, N. P. (2022). The role of subsidence and accommodation generation in controlling the nature of the aeolian stratigraphic record. *J. Geol. Soc.* 179, jgs2021–2042. doi:10.1144/jgs2021-042
- Deng, G., Xie, Y., Yang, G., Wang, J., Jiang, X., Li, M., et al. (2008). Characteristics of cretaceous aquifer sandstone in the Ordos Basin. *Acta Geol. Sichuan* 28, 124–130. doi:10.3969/j.issn.1006-0995.2008.02.012
- Dong, Y., Zhang, G., Neubauer, F., Liu, X., Genser, J., and Hauzenberger, C. (2011). Tectonic evolution of the Qinling orogen, China: Review and synthesis. *J. Asian Earth Sci.* 41, 213–237. doi:10.1016/j.jseas.2011.03.002
- Dong, Z., Qian, G., Luo, W., Zhang, Z., Xiao, S., and Zhao, A. (2009). Geomorphological hierarchies for complex mega-dunes and their implications for mega-dune evolution in the Badain Jaran Desert. *Geomorphology* 106, 180–185. doi:10.1016/j.geomorph.2008.10.015
- Du, H., Hasi, E., Lei, J., and Yang, Y. (2013). A study of morphological change of parabolic dune in Hobq Desert based on 3S technology. *Bull. Soil Water Conservation* 33, 165–169.
- Du, H., Hasi, E., Wu, X., Yang, Y., and Eriduntonglaga, Y. (2011). Application of 3S technology in morphological character research of parabolic dune. *Geogr. Geo - Inf. Sci.* 27, 33–36.
- Ewing, R. C., and Kocurek, G. (2010). Aeolian dune-field pattern boundary conditions. *Geomorphology* 114, 175–187. doi:10.1016/j.geomorph.2009.06.015
- Fan, Y., Chen, X., Fan, T., Jin, M., Liu, J., and Chen, F. (2013). Sedimentary and OSL dating evidence for the development of the present Hobq desert landscape, northern China. *Sci. China Earth Sci.* 56, 2037–2044. doi:10.1007/s11430-013-4673-7
- He, Z., Zhou, J., Lai, Z., Yang, L., Liang, J., Long, H., et al. (2010). Quartz OSL dating of sand dunes of late Pleistocene in the Mu us Desert in northern China. *Quat. Geochronol.* 5, 102–106. doi:10.1016/j.quageo.2009.02.011
- Hesp, P. A., and Hastings, K. (1998). Width, height and slope relationships and aerodynamic maintenance of barchans. *Geomorphology* 22, 193–204. doi:10.1016/s0169-555x(97)00070-6
- Howell, J., and Mountney, N. (2001). Aeolian grain flow architecture: Hard data for reservoir models and implications for red bed sequence stratigraphy. *Pet. Geosci.* 7, 51–56. doi:10.1144/petgeo.7.1.51
- Huang, Y. (2010). *The origin and evolution of the desert in southern Ordos in early Cretaceous: Constraint from magnetostratigraphy of Zhidan Group and magnetic susceptibility of its sediment*. Lanzhou, China: Lanzhou University.
- Huang, Y., Wang, N.-a., He, T., Chen, H., and Zhao, L. (2009). Historical desertification of the Mu Us Desert, northern China: A multidisciplinary study. *Geomorphology* 110, 108–117. doi:10.1016/j.geomorph.2009.03.020
- Jiang, X., Pan, Z., and Fu, Q. (2001). Regularity of paleowind directions of the early cretaceous Desert in Ordos Basin and climatic significance. *Sci. China Ser. D Earth Sci.* 44, 24–33. doi:10.1007/bf02906882
- Jiang, X., Pan, Z., Xie, Y., and Li, M. (2004). Cretaceous desert cycles, wind direction and hydrologic cycle variations in Ordos Basin: Evidence for Cretaceous climatic unequability. *Sci. China Ser. D Earth Sci.* 47, 727–738. doi:10.1360/02yd0031
- Laity, J. J. (2009). *Deserts and desert environments*. New Jersey, United States: John Wiley & Sons.
- Lancaster, N. (1994). Controls on aeolian activity: Some new perspectives from the kelso dunes, mojave desert, California. *J. Arid Environ.* 27, 113–125. doi:10.1006/jare.1994.1052
- Li, S., Guo, L., Xu, L., Somerville, I. D., Cao, X., Yu, S., et al. (2015). Coupling and transition of meso-cenozoic intracontinental deformation between the Taihang and qinling mountains. *J. Asian Earth Sci.* 114, 188–202. doi:10.1016/j.jseas.2015.04.011
- Li, X., Dong, G., Jin, H., Su, Z., and Wang, Y. (1999). Discovery of Ordos Cretaceous dune rock and its significance. *Chin. Sci. Bull.* 44, 2102–2106. doi:10.1007/bf02884931
- Liu, Q., and Yang, X. (2018). Geochemical composition and provenance of aeolian sands in the Ordos Deserts, northern China. *Geomorphology* 318, 354–374. doi:10.1016/j.geomorph.2018.06.017
- Liu, X., Lu, R., Du, J., Lyu, Z., Wang, L., Gao, S., et al. (2018). Evolution of peatlands in the Mu Us Desert, northern China, since the last deglaciation. *J. Geophys. Res. Earth Surf.* 123, 252–261. doi:10.1002/2017jef004413
- Lu, H., Wang, X., Wang, X., Chang, X., Zhang, H., Xu, Z., et al. (2019). Formation and evolution of gobi Desert in central and eastern Asia. *Earth-Science Rev.* 194, 251–263. doi:10.1016/j.earscirev.2019.04.014
- Lü, T., Sun, J., Feathers, J. K., and Sun, D. (2020). Spatiotemporal variations and implications of luminescence sensitivity of quartz grains on the Chinese Loess Plateau since the last interglaciation. *Quat. Res.* 99, 190–203. doi:10.1017/qua.2020.53
- Ma, J., Cao, S., Zhang, Z., and Wang, C. (2021). Quantitative reconstruction of ancient dunes morphology in palaeo-deserts. *J. Shandong Univ. Sci. Technol. Nat. Sci.* 40, 10–22.
- Meinshausen, M., Nicholls, Z. R., Lewis, J., Gidden, M. J., Vogel, E., Freund, M., et al. (2020). The shared socio-economic pathway (SSP) greenhouse gas concentrations and their extensions to 2500. *Geosci. Model Dev.* 13, 3571–3605. doi:10.5194/gmd-13-3571-2020
- Mirzabae, A., Wu, J., Evans, J., Garcia-Oliva, F., Hussein, I. A. G., Iqbal, M. H., et al. (2019). "Desertification," in *Climate change and land: An IPCC special report on climate change, desertification, land degradation, sustainable land management, food security, and greenhouse gas fluxes in terrestrial ecosystems*. Editors P. R. Shukla, J. Skeg, E. Calvo Buendia, V. Masson-Delmotte, H. O. Pörtner, D. C. Roberts, et al. (Geneva, Switzerland: Intergovernmental Panel on Climate Change).
- Mountney, N., and Howell, J. (2000). Aeolian architecture, bedform climbing and preservation space in the Cretaceous Etjo Formation, NW Namibia. *Sedimentology* 47, 825–849. doi:10.1046/j.1365-3091.2000.00318.x
- Mountney, N. P. (2012). A stratigraphic model to account for complexity in aeolian dune and interdune successions. *Sedimentology* 59, 964–989. doi:10.1111/j.1365-3091.2011.01287.x
- Mountney, N. P. (2006). "Eolian facies models," in *Facies models revisited*. Editors H. W. Posamentier (Tulsa, Oklahoma: Society for Economic Paleontologists and Mineralogists), 19–83.
- O'Brien, C. L., Robinson, S. A., Pancost, R. D., Sinninghe Damsté, J. S., Schouten, S., Lunt, D. J., et al. (2017). Cretaceous sea-surface temperature evolution: Constraints from TEX86 and planktonic foraminiferal oxygen isotopes. *Earth-Science Rev.* 172, 224–247. doi:10.1016/j.earscirev.2017.07.012
- Pan, Y., and Huang, C. (2014). Quantitative reconstruction of early cretaceous paleoclimate using paleosol carbonates in China. *Carbonates Evaporites* 29, 327–335. doi:10.1007/s13146-013-0184-z

- Pastore, G., Baird, T., Vermeesch, P., Bristow, C., Resentini, A., and Garzanti, E. (2021). Provenance and recycling of Sahara Desert sand. *Earth-Science Rev.* 216, 103606. doi:10.1016/j.earscirev.2021.103606
- Pörtner, H.-O., Roberts, D. C., Adams, H., Adler, C., Aldunce, P., Ali, E., et al. (2022). *Climate change 2022: Impacts, adaptation and vulnerability*. Geneva, Switzerland: IPCC Sixth Assessment Report.
- Pye, K. (2009). *Aeolian sand and sand dunes*. Berlin, Germany: Springer.
- Qi, H., and Li, G. (1996). The systems of palaeodesert basins in sedimentary period of Zhidan Group, Ordos Basin. *Northwest Geosci.* 17, 63–90.
- Qiao, D., Peng, N., Kuang, H., Liu, Y., Liu, Y., Cui, L., et al. (2021). Changes in prevailing surface-paleowinds reveal the atmospheric circulation transition during Early Cretaceous in North China: *Palaeogeogr. Palaeoclimatol. Palaeoecol.*, 586, 110784. doi:10.1016/j.palaeo.2021.110784
- Ren, X., Liu, T., and Zhenting, W. (2010). Characters of geomorphologic parameter about banchan dunes. *Res. Soil Water Conservation* 17, 163–166.
- Rittner, M., Vermeesch, P., Carter, A., Bird, A., Stevens, T., Garzanti, E., et al. (2016). The provenance of Taklamakan desert sand. *Earth Planet. Sci. Lett.* 437, 127–137. doi:10.1016/j.epsl.2015.12.036
- Rodríguez-López, J. P., Clemmensen, L. B., Lancaster, N., Mountney, N. P., and Veiga, G. D. (2014). Archean to Recent aeolian sand systems and their sedimentary record: Current understanding and future prospects. *Sedimentology* 61, 1487–1534. doi:10.1111/sed.12123
- Romain, H. G., and Mountney, N. P. (2014). Reconstruction of three-dimensional eolian dune architecture from one-dimensional core data through adoption of analog data from outcrop. *AAPG Bull.* 98, 1–22. doi:10.1306/05201312109
- Rubin, D. M., and Carter, C. L. (2006). *Cross-bedding, bedforms, and paleocurrents*. Tulsa, Oklahoma: Society for Sedimentary Geology.
- Shi, W., Dong, S., and Hu, J. (2020). Neotectonics around the Ordos Block, north China: A review and new insights. *Earth-Science Rev.* 200, 102969. doi:10.1016/j.earscirev.2019.102969
- Stevens, T., Palk, C., Carter, A., Lu, H., and Cliff, P. D. (2010). Assessing the provenance of loess and desert sediments in northern China using U-Pb dating and morphology of detrital zircons. *GSA Bull.* 122, 1331–1344. doi:10.1130/b30102.1
- Sun, J., Li, S.-H., Han, P., and Chen, Y. (2006). Holocene environmental changes in the central Inner Mongolia, based on single-aliquot-quartz optical dating and multi-proxy study of dune sands. *Palaeogeogr. Palaeoclimatol. Palaeoecol.* 233, 51–62. doi:10.1016/j.palaeo.2005.09.016
- Sun, J. (2000). Origin of eolian sand mobilization during the Past 2300 Years in the Mu Us Desert, China. *Quat. Res.* 53, 78–88. doi:10.1006/qres.1999.2105
- Tierney, J. E., Poulsen, C. J., Montañez, I. P., Bhattacharya, T., Feng, R., Ford, H. L., et al. (2020). Past climates inform our future. *Science* 370, eaay3701. doi:10.1126/science.aay3701
- Wang, J., Liu, L., and Shen, L. (2013). Research of the barchan dunes movement in the Mu Us sandy land on Google Earth software. *Remote Sens. Technol. Appl.* 28, 1094–1100.
- Wang, X., Cheng, H., Li, H., Lou, J., Hua, T., Liu, W., et al. (2017). Key driving forces of desertification in the Mu Us Desert, China. *Sci. Rep.* 7, 3933. doi:10.1038/s41598-017-04363-8
- Xiao, J., Xie, X., Zhao, H., Chen, C., Ma, X., Qu, J., et al. (2021). Seasonal changes and migration of longitudinal dunes in the northeastern Rub'al Khali Desert. *Aeolian Res.* 51, 100710. doi:10.1016/j.aeolia.2021.100710
- Xiao, T. (2017). *A study of dune morphology and its evolution based on high resolution remote sensing data*. Hunan, China: Hunan Normal University, 65.
- Xiao, W., Windley, B. F., Han, C., Liu, W., Wan, B., Zhang, J. e., et al. (2018). Late Paleozoic to early Triassic multiple roll-back and oroclinal bending of the Mongolia collage in Central Asia. *Earth-Science Rev.* 186, 94–128. doi:10.1016/j.earscirev.2017.09.020
- Xing, L., Lockley, M. G., Tang, Y., Romilio, A., Xu, T., Li, X., et al. (2018). Tetrapod track assemblages from lower Cretaceous desert facies in the Ordos Basin, shaanxi province, China, and their implications for mesozoic paleoecology. *Palaeogeogr. Palaeoclimatol. Palaeoecol.* 507, 1–14. doi:10.1016/j.palaeo.2018.05.016
- Xu, M., Lü, P., Xiao, N., Yang, J., Liu, Z., Feng, M., et al. (2020). Effect of vegetation cover on dune migration in northwest Mu Us sandy land. *J. Desert Res.* 40, 71–80. doi:10.7522/j.issn.1000-694X.2020.00020
- Xu, Y., Lai, Z., Chen, T., and Gong, S. (2018). Late Quaternary optically stimulated luminescence (OSL) chronology and environmental changes in the Hobq Desert, northern China. *Quat. Int.* 470, 18–25. doi:10.1016/j.quaint.2017.06.010
- Xue, C., Chi, G., and Xue, W. (2010). Interaction of two fluid systems in the formation of sandstone-hosted uranium deposits in the Ordos Basin: Geochemical evidence and hydrodynamic modeling. *J. Geochem. Explor.* 106, 226–235. doi:10.1016/j.jexplo.2009.11.006
- Yang, H., Cao, J., and Hou, X. (2019). Characteristics of aeolian dune, wind regime and sand transport in Hobq Desert, China. *Appl. Sci.* 9, 5543. doi:10.3390/app9245543
- Yang, J., Dong, Z., Liu, Z., Shi, W., Chen, G., Shao, T., et al. (2019). Migration of barchan dunes in the Western Quruq Desert, northwestern China. *Earth Surf. Process. Landforms* 44, 2016–2029. doi:10.1002/esp.4629
- Yang, L., Shi, Z., Sun, H., Xie, X., Liu, X., and An, Z. (2021). Distinct effects of winter monsoon and westerly circulation on dust aerosol transport over East Asia. *Theor. Appl. Climatol.* 144, 1031–1042. doi:10.1007/s00704-021-03579-z
- Yang, L., Zou, N., Yue, L., and Guo, H. (2017). Distribution of U-Pb ages of detrital zircon from the Hobq Desert and its implications for provenance. *Quat. Sci.* 37, 560–569. doi:10.11928/j.issn.1001-7410.2017.03.12
- Yang, X., and Dong, Y. (2018). Mesozoic and cenozoic multiple deformations in the helanshan tectonic belt, northern China. *Gondwana Res.* 60, 34–53. doi:10.1016/j.gr.2018.03.020
- Yang, X., Forman, S., Hu, F., Zhang, D., Liu, Z., and Li, H. (2016). Initial insights into the age and origin of the Kubuqi sand sea of northern China. *Geomorphology* 259, 30–39. doi:10.1016/j.geomorph.2016.02.004
- Yang, X., Li, H., and Conacher, A. (2012). Large-scale controls on the development of sand seas in northern China. *Quat. Int.* 250, 74–83. doi:10.1016/j.quaint.2011.03.052
- Yu, X., Zhuo, Y., Liu, H., Wang, Q., Wen, L., Li, Z., et al. (2020). Degree of desertification based on normalized landscape index of sandy lands in inner Mongolia, China. *Glob. Ecol. Conservation* 23, e01132. doi:10.1016/j.gecco.2020.e01132
- Zhang, C., Shen, Y., Li, Q., Jia, W., Li, J., and Wang, X. (2018). Sediment grain-size characteristics and relevant correlations to the aeolian environment in China's eastern desert region. *Sci. Total Environ.* 627, 586–599. doi:10.1016/j.scitotenv.2018.01.270
- Zhang, C. (2019). *Study on dune morphological characteristics of different measures based on unmanned aerial vehicle technology*. Inner Mongolia, China: Inner Mongolia Agricultural University, 61.
- Zhang, Z., Wang, T., Ramezani, J., Lv, D., and Wang, C. (2020). Climate forcing of terrestrial carbon sink during the middle jurassic greenhouse climate: Chronostratigraphic analysis of the yan'an formation, Ordos Basin, north China. *GSA Bull.* 133, 1723–1733. doi:10.1130/b35765.1
- Zhao, J., Liu, C., Huang, L., Zhang, D., Wang, D., and Wang, D. (2020). Paleogeography reconstruction of a multi-stage modified intra-cratonic basin—A case study from the jurassic Ordos Basin, Western north China craton. *J. Asian Earth Sci.* 190, 104191. doi:10.1016/j.jseas.2019.104191
- Zhu, B., Zhang, J., and Sun, C., (2021). Physiochemical characteristics, provenance, and dynamics of sand dunes in the arid hexi corridor. *Frontiers in Earth Science*, 9, 726. doi:10.3389/feart.2021.728202
- Zhu, X., Liu, L., Jia, S., Rui-qi, L., and Gong, Y.-d. (2018). Geochemical and provenance characteristics of eolian sandstone of cretaceous Luohe Formation in Ordos basins: An example from outcrop in longzhou, jingbian. *Glob. Geol.* 37, 702–711.
- Zonn, I. S., and Esenov, P. E. (2012). *The turkmen lake altyn asyr and water resources in Turkmenistan*. Berlin, Germany: Springer, 23–37. The Karakum Desert.